Archives of Civil and Mechanical Engineering (2022) 22:153
https://doi.org/10.1007/s43452-022-00476-8

ORIGINAL ARTICLE

Heat treatment of bimetals produced by selective laser melting of MS1 maraging steel on conventionally produced 42SiCr martensitic steel

Ludmila Kučerová[1] · Štěpán Jeníček[1] · Ivana Zetková[1] · Karolína Burdová[1]

Received: 19 January 2022 / Revised: 19 May 2022 / Accepted: 12 June 2022

Abstract
One approach to producing hybrid bimetallic parts is to additively manufacture a new material onto a conventionally manufactured base material. This technique can expand the potential applications of additive manufacturing and offer new solutions for the engineering design of hybrid parts. In this work, laser powder bed fusion was used to deposit MS1 maraging steel on a conventionally produced (cast and hot-rolled) 42SiCr martensitic steel base material. Despite the profoundly different chemical compositions and hardening behaviours of these materials, their yield and ultimate tensile strengths in solution-annealed and hardened conditions are quite similar. Various heat treatments were performed to optimise the mechanical properties of the resulting hybrid part. The highest yield strength of 1400 MPa and tensile strength of 1483 MPa was achieved with a post-processing heat treatment which consisted of annealing at 900 °C for 25 min followed by water quenching and subsequent very short tempering at 490 °C. In the tensile tests, all the hybrid parts, regardless of heat treatment parameters, fractured within the base material and neither in the joint nor in the adjacent heat-affected zone. The interface areas and the microstructures of both materials were documented in detail in the as-built state and also after the heat treatment.

Keywords Hybrid part · Maraging steel · High strength steel · Powder bed fusion · Selective laser melting

1 Introduction

Additive manufacturing (AM) is a continuously growing and developing sector which consists of many technologies dedicated to the manufacture of particular materials or to specific applications. Among the most popular metal additive manufacturing processes are various laser-based methods, namely powder bed fusion and direct deposition technologies. Powder bed technologies such as direct metal laser sintering (DMLS) or selective laser melting (SLM) are often used for additive manufacturing of steels, specifically 18Ni-300 maraging steel [1–4] or 316 L stainless steel [5–7]. Early research focused on the relationship between process parameters and porosity, microstructure and basic mechanical properties of the builds [1–8]. The many works dealing with SLM maraging steel include the analyses of the effect of two scan directions on the tensile properties of maraging steel [1], suggesting that the most suitable direction is 90°; the study of the position of a sample on the building platform in relation to its microstructure and surface quality [2]; the relationship between the thickness of the powder layer and the resulting mechanical properties [3]; or a description of the effect of printing defects on fracture initiation [4]. Similar problems were also studied for SLM stainless steel, ranging from the effect of build orientation [5], or detailed analysis of printing defects [6], to complex optimization of process parameters and their effect on microstructure in [7].

Later, post-processing treatments of AM steels and more comprehensive material characterisation began to be explored. These included the combination of the effects of various printing directions and heat treatments on the microstructure and mechanical properties of maraging steel [8], fatigue properties [9], changes of mechanical properties introduced by environmental exposure [10], and microstructure features connected with heat treatment such as precipitation and strengthening [11], austenite reversion and stability [12] and a combination of all these features in a wide interval of heat treatment conditions [13].

Recently, several studies have looked at the development of systems and parts containing dissimilar joints of several metals, bimetallics, or functionally graded materials with

✉ Ludmila Kučerová
skal@rti.zcu.cz

[1] Regional Technological Institute, University of West Bohemia, Univerzitni 8, 301 00 Pilsen, Czech Republic

Published online: 04 July 2022

continuously varying chemical compositions, rather than the additive manufacturing of a single material [14–17]. The application of LSM produced hybrid parts in tooling was suggested in [14] aimed at maraging steel-H13 steel hybrid parts, and also in [15] which concentrated on heat treatment of the same maraging steel-H13 steel hybrid part. SLM hybrid parts of maraging steel-advanced high strength steel and the effect of their heat treatment on their mechanical properties was described in [16].The possibility of using wire arc additive manufacturing for production of low carbon—stainless steel hybrid parts was also reported in [17].

This trend fully exploits the advantages of additive manufacturing, leading to innovative material concepts, which challenge existing practices and designs. Another way to develop hybrid bimetallic parts is to combine additive manufacturing with conventional technologies to obtain new products. Combinations of SLM additive and subtractive technologies (machining) of AlSi10Mg alloy have already been proposed in this context [18]. However, current attempts to produce hybrid parts by AM on forged semi-products are quite rare and mainly concentrate on hybrid parts created by various technologies from a single or very similar material. For example, SLM deposition of AISI 630 on point incremental formed sheets of AISI 304 was successfully carried out in [19], forging and wire arc additive manufacturing of AlSi1MgMn alloy was performed in [20], and SLM of Ti-6Al-4V alloy on a forged semi-product of the same chemical composition was reported in [21] and the application of a Ti6al4V hybrid part in aerospace components was described in [22].

Most studies on the preparation of dissimilar hybrid or bimetallic materials using powder-based methods focus on direct deposition technologies, such as dissimilar alloy walls fabricated from A410L, A316-L stainless steels and zirconium [23], or deposition of AISI 316 stainless steel on Ti6al4V substrate [24]. One of the powderless technologies which has recently been used for this purpose is wire arc additive manufacturing, which was used to produce hybrid parts from Ni6082 alloy and YS308L stainless steel [25], Ti6Al4V and AlSi5 alloys [26], and 309L stainless steel and mild steel [27].

Direct deposition processes (DDP) are generally believed to be better suited for this innovative approach than powder bed technologies because DDPs can deposit materials on substrates of various shapes. With the powder bed AM process, a new layer can only be built on a planar surface, which could present serious limitations in practical applications. However, powder bed technologies are considered to achieve better product accuracy than direct deposition, which could also be an important aspect [28]. Up to now, only a few attempts at using powder bed AM for steel deposition on conventional materials have been published. Besides the maraging steel mentioned above—H13 steel hybrid parts [14, 15, 17], which were also investigated in [29], maraging steel-copper bimetals were also produced [30]. However, a very limited selection of substrate materials has been investigated and with various degrees of success, which leaves a large field open for further research. This study investigates the production of a hybrid part made from AM maraging steel and conventionally produced medium-carbon low-alloyed martensitic steel, which would have good mechanical properties as a result of post-processing heat treatment. Selective laser melting was used to build a hybrid part by depositing 18Ni-300 maraging steel onto hot-rolled 42SiCr martensitic steel. A post-processing heat treatment was designed to give the hybrid part good mechanical properties by balancing the properties of the maraging steel and 42SiCr steel.

18Ni-300 is a typical maraging steel which can be used in hot injection moulding of plastics or in the casting of non-ferrous metals. It is also frequently applied in the automotive or aerospace industry due to its good strength to weight ratio, which makes it suitable for the production of safety–critical parts. In all these applications, it would be advantageous to combine it with less alloyed, and, therefore, less expensive, high strength 42SiCr martensitic steel. 42SiCr steel is a chromium alloyed medium-carbon steel resembling H13 steel, but with a significantly lower amount of alloying elements. It has good formability and can be easily processed by various technologies into sheets, bulk or rotationally symmetrical semi-products and its application range is very similar to that of 18Ni-300 steel. This supports the idea of joining both steels into a single hybrid part. The medium-carbon content of 42SiCr steel causes its lower weldability and, therefore, deposition of 18Ni-300 steel on its surface does present a welcome option for the production of heterogeneous joints. An additional advantage of these hybrid parts is the possibility to create innovative designs or more complex inner shapes on the AM side of the part, such as more efficient cooling systems in moulds, or various lightweight structures in structural parts. Both steels have similar tensile strengths of approximately 1000 MPa when annealed and around 2000 MPa when hardened, as was reported for maraging steel [4] and also 42SiCr steel [31] after heat treatments. They also both could contain small fractions of retained or reverted austenite (RA) in the final microstructure. However, a major difference between them is their hardening mechanisms.

On quenching, medium-carbon 42SiCr steel develops super-saturated martensite, the properties of which can be adjusted by tempering, which leads to the migration of excess carbon and the formation of carbides. The higher the tempering temperature, the lower the final tensile strength and the greater the elongation. Alternatively, this steel can be treated using the quenching and partitioning (QP) process which was introduced by Speer et al. [32], which can further

improve ductility and toughness of low-to-medium carbon steels without compromising strength. The effect of the QP process on the mechanical properties of high strength steels has been demonstrated on a high-silicon medium-carbon steel of similar chemical composition to 42SiCr by [33], various low-carbon-low-alloyed steels by [34], medium manganese steels by [35] and finally also directly on heat treated 42SiCr steel [36].

By contrast, the maraging steel investigated in this study is practically carbon-free. Precipitation of fine intermetallic particles is, therefore, the basis of its hardening. Precipitation intensifies with increasing hardening temperature, leading to higher strength, with the peak hardness achieved after hardening at approximately 490 °C [12].

Put simply, the strength of 42SiCr steel generally decreases with increasing tempering temperature, whereas the opposite trend occurs in maraging steel. Hence, optimal tempering/hardening conditions need to be identified for a hybrid part made from these two steels to obtain good and evenly distributed strength in both materials.

2 Experimental procedures

2.1 Materials

Two different steels were used for these experiments: martensitic 42SiCr steel and maraging steel 18Ni-300 (Table 1). Medium carbon 42SiCr low-alloyed tool steel was developed primarily for the quenching and partitioning process, where the effects of various cooling strategies and quenching temperatures [31] and partitioning temperatures and holds [36] on mechanical properties have already been tested. This steel is not governed by any conventional standard, and it was custom cast in a vacuum induction furnace. The ingot was then cut into sections and hot-rolled at 1050 °C into 11 mm thick plates. The plates were further homogenized for 4 h at 1100 °C and used for making cylindrical stock. Samples with a diameter of 10 mm and a height of 45 mm were prepared for the experiments. Their initial microstructure was pearlitic with a small fraction of ferrite at the prior austenite grain boundaries. Their hardness was 281 HV10.

The second material was maraging steel powder X3NiCoMoTi 18-9-5, equivalent to 1.2709 grade and 18Ni-300 grade. The commercial name of the powder is MS1 and it was obtained from the company EOS. Detailed characterisation of the powder, such as average powder size, microstructure and chemical composition are given for a virgin powder in [17] and for the virgin and also re-used powder in [37]. The average powder particle size was evaluated repeatedly for several batches using image analysis. In all cases, the values were very similar, approximately 25 µm [37].

2.2 Processing

2.2.1 Additive manufacturing

The MS1 maraging steel was deposited using an EOS M290 additive manufacturing machine in a protective nitrogen gas atmosphere. The processing parameters followed the recommendations of the powder and printing machines supplier for maraging steel. The layer thickness was 40 µm. A laser power of 258 W was applied at a scanning rate of 960 mm/s. The laser spot size was 80 µm. The hatch spacing was 110 µm and a misorientation angle of 67° was applied. The greatest difficulty when producing these hybrid parts was ensuring the precise positioning of the 42SiCr stock on the base plate and keeping the surfaces planar and parallel to the blade edge of the recoating device. The cylinders were, therefore, threaded at one end and screwed into holes in the base plate (Fig. 1). The tops of all the mounted cylinders were then ground at the same time to ensure their even height above the base plate which was necessary for a successful deposition. Details of this adjustment process are given in [17].

2.2.2 Heat treatment

A reference hybrid sample was produced and examined in the as-fabricated condition, without post-processing heat treatment, to observe the results of the deposition of MS1 on 42SiCr steel (Table 2). Conventional quenching and tempering of 42SiCr steel results in an ultimate tensile strength of around 1800–2000 MPa and 8–10% total elongation [36]. These properties are comparable with precipitation hardened 18Ni-300 steel, which typically has a tensile strength in the region of 1800–2100 MPa in solution annealed and peak hardened condition and 4–6% total elongation.

All the other hybrid samples were subjected to various heat treatments to optimise the mechanical properties of the entire hybrid part. The heat treatment was done in an argon atmosphere to protect the surfaces of the part, particularly the 42SiCr side, which is more prone to oxidation than the

Table 1 Chemical composition of the experimental materials (weight %)

	C	Si	Mn	Cr	Nb	Ni	Mo	Ti	Co
42SiCr	0.4	2.0	0.6	1.3	0.03	–	–	–	–
MS1	0.001	0.02	0.02	–	–	17.7	4.9	0.8	8.7

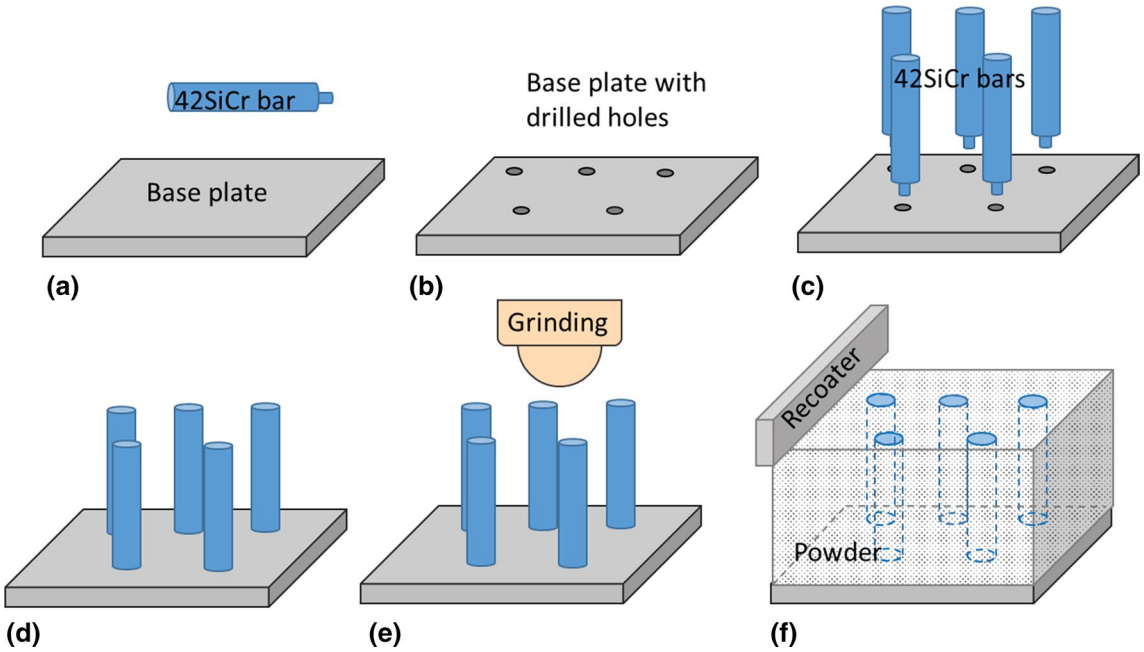

Fig. 1 Schematic of the preparation process for selective laser melting of MS1 maraging steel on 42SiCr martensitic steel. **f** shows the state in the chamber just before the additive manufacturing of MS1 started

Table 2 Post-processing heat treatments for hybrid parts

Sample No	Post-processing heat treatment
1-without HT	Without heat treatment (HT)
2-QT-250 °C/2 h	900 °C/25 min, water quenched to RT, 250 °C/2 h
5-QT-490 °C/0 h	900 °C/25 min, water quenched to RT, 490 °C/0 h
6-QT-490 °C/6 h	900 °C/25 min, water quenched to RT, 490 °C/6 h

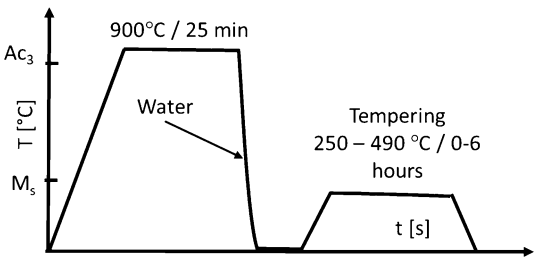

Fig. 2 Post-process heat treatment schedules

maraging steel. A soaking temperature of 900 °C was used for all the treatments, as it is suitable for both steels.

Following this, quenching and tempering (QT) was applied (Fig. 2). The tempering temperatures and times were varied from 250 to 490 °C and from 0 to 6 h. The interval of the tempering temperatures was set from the tempering temperature of 250 °C, commonly used for 42SiCr steel, to the tempering temperature of 490 °C, which is typically used for precipitation hardening of maraging steel. Finally, all the parts were left to cool in air to room temperature (RT). When a hold is identified as "0" hours, it means that the part was only brought to the given temperature. Once this temperature was reached in the whole of the part (according to the inserted thermocouple), it was removed from the furnace and cooled in air.

2.3 Characterisation

Longitudinal metallographic sections were prepared from the hybrid parts to characterise the microstructure at the 42SiCr-maraging steel interface. The side cross-section (build direction) was observed in AM steel and the rolling direction in 42SiCr steel. The samples were prepared by standard grinding and polishing and etched with 3% nital. General images were taken using a BX61 Olympus light microscope. Microstructure details and fracture surfaces after tensile testing were documented using a high resolution scanning electron microscope (HR-SEM) Crossbeam Auriga with energy-dispersive X-ray spectroscopy (EDS) and electron backscattered diffraction (EBSD) detectors. Light and scanning electron microscopy were applied to all samples, selected results showing typical microstructure features are presented in the images accompanying this article. An AXS Bruker D8 Discover diffractometer with a Co source was used for X-ray diffraction phase analysis of the volume fraction of retained austenite in the AM maraging steel. The amount of retained austenite was quantified from (111), (002) and (022) peak intensities.

Hardness and tensile tests were chosen as the initial methods for characterisation of the mechanical properties of the hybrid parts. This does not mean that the practical applications of these hybrid parts would not require the determination of other mechanical properties as well, such as fatigue or thermo-mechanical fatigue. However, starting with hardness and tensile tests seemed the most practical option for several reasons. First, hardness is commonly used in industrial practice as the initial value for assessing the properties of processed materials and also for characterising welds and joints. Second, tensile test results are also generally expected for any new material solutions and all these values are easily comparable with previously published results from hybrid parts and bimetals (which also nearly exclusively focus on hardness and tensile tests) and with material standards. They are also important for various numerical simulations dealing with the expected behaviour of the hybrid part in particular loading conditions. And finally, the chosen methods allow for a quick and standard evaluation of the effects of heat treatment on the properties of the hybrid parts and could, therefore, be used as the first step to eliminate the less well-performing options.

A Zwick Roller Z250 testing machine was used to perform tensile tests at a strain rate of 0.0067 s^{-1} according to EN ISO 6892-1. Two tensile specimen geometries were used. First, specimens with a circular cross-section and 20 mm gauge length, 4 mm diameter, and M8-threaded head were produced from the entire hybrid parts. In these specimens, the 42SiCr-MS1 interface was located in the middle of the sample (Fig. 3a). In addition, three small flat samples (mini-samples) with a cross-section of 2 × 1.2 mm and a gauge length of 5 mm were extracted from each side of the hybrid part (Fig. 3b). Therefore, there were three flat samples of 42SiCr steel and three flat samples of MS1 steel. This set of specimens allowed us to determine the effect of post-processing heat treatment on the mechanical properties of both steels as well as on the whole hybrid part. However, due to the different geometries of the flat and round test specimens, the data were not exactly comparable, particularly for elongation.

The hardness HV10 of both materials was measured using a Wolpert 432-SVD hardness tester. Average hardness was calculated from 3 imprints. A Leco LM248 AT device was used to map the microhardness around the interface by producing an array of 240 imprints on the polished surface. Etching would obscure the edges of the imprints and preclude automatic evaluation. A load of 100 g (HV 0.1) was applied with 0.05 mm spacing between the imprints. Hardness maps were then exported and aligned with light micrographs taken after slight etching of the indented sample. Microhardness could thus be correlated with the local microstructure and the distance from the 42SiCr-MS1 interface.

3 Results and discussion

3.1 Microstructure

In all the builds, the quality of the 42SiCr-MS1 interface was good, without visible porosity or lack of fusion (Fig. 4). However, a distinct diffusion interlayer at the interface was observed where the steels were mixed. It is visible in the micrographs, and is due to the mixed microstructures differing from the base microstructures of each steel.

3.1.1 Hybrid part without post-processing heat treatment

The reference hybrid sample, which did not undergo any post-processing heat treatments, had a pearlitic microstructure with a small amount of ferrite on the 42SiCr side and a cellular microstructure typical for as-built maraging steel on the MS1 side (Fig. 5a). Around 3% of retained austenite was detected in the maraging steel, which had already been located at the cell boundaries with a higher concentration of alloying elements [4]. However, this kind of cell microstructure was not observed in conventionally solution-annealed maraging steel where lath martensite with a more homogeneous distribution of alloying elements and no retained austenite would be expected. Additionally, the AM maraging steel used in this study also contains very fine globular Ti–Al–O particles and rhombus-shaped Ti–Al–N particles, as was reported previously for samples printed with the same parameters [13]. The 42SiCr-MS1 steel interface was clearly visible in the micrographs due to dissimilar microstructures (Fig. 4). However, it was not a sharp boundary, even at higher magnifications (Fig. 5b, d, e). The materials were intermixed by circular flow [29, 30]. Even though intensive diffusion occurred at the interface, two different types of areas could be still distinguished on the micrographs. The distribution of individual elements in Fig. 5b shows that "smoother" looking areas contain high concentrations of the main alloying elements of MS1 steel, such as nickel, cobalt

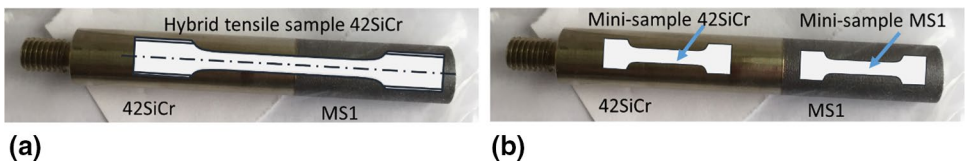

Fig. 3 Position of **a** cylindrical hybrid samples and **b** flat mini-samples of each material for tensile testing

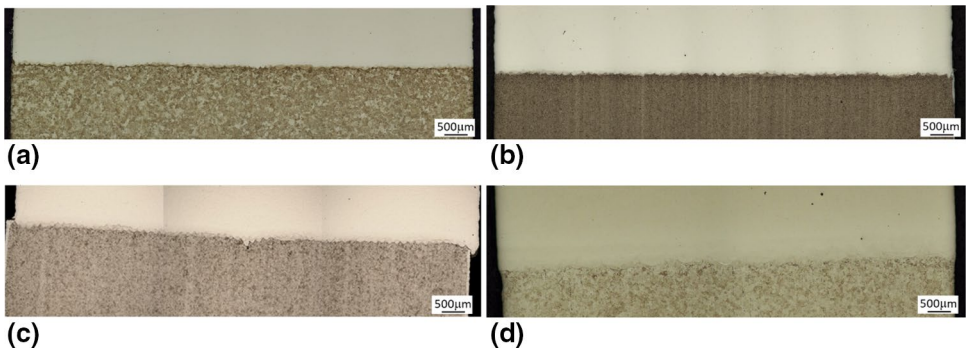

Fig. 4 General view of the interface region in sample 1-without HT **a** 2-QT-250 °C/2 h **b**, 3-QT-490 °C/0 h **c** and 4-QT-490 °C/6 h **d**. Maraging steel is at the top of the micrograph and 42SiCr steel is at the bottom. Due to different etch-ability of the steels, the 42SiCr part is already distinctively etched while no microstructure features are yet visible in the maraging steel part (the interface is invisible in the polished state without etching)

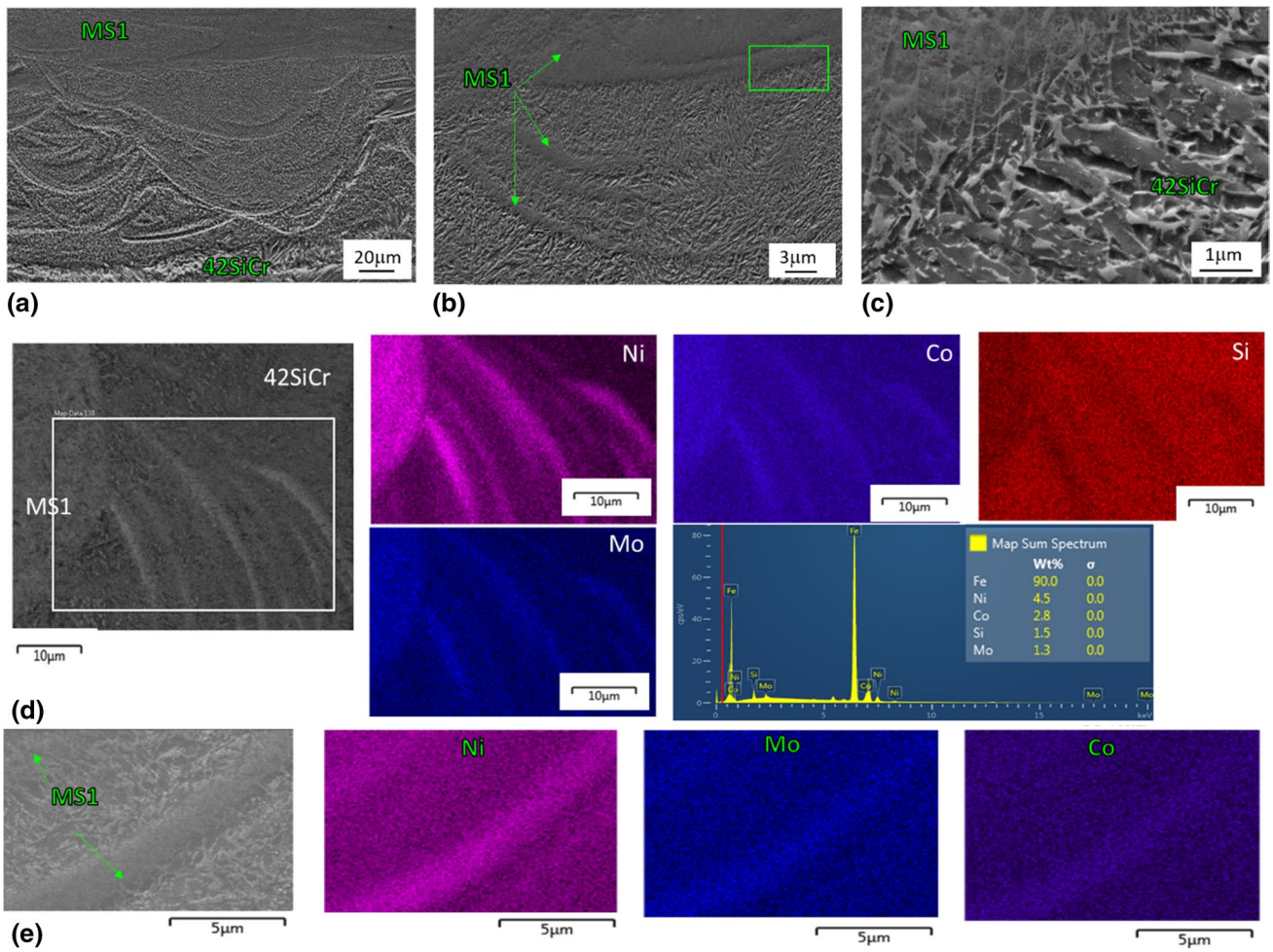

Fig. 5 Microstructure of the reference hybrid sample which received no post-process heat treatment 1-without HT: **a**, **b** Microstructure of the interface with increasing magnification, c) detail of the interface marked by green rectangle in **b**, **d** element mapping of the larger area of the interface, **e** element mapping of the interface in detail

and molybdenum. Those areas could be further described as corresponding to MS1 steel, while the more etched areas between them have a chemical composition closer to the 42SiCr steel. The interface microstructure of the areas with a chemical composition mainly corresponding to 42SiCr resembled lower bainite, with thin films of retained austenite along plate boundaries (Fig. 5c). There was no pearlite or proeutectoid ferrite in areas where the chemical composition was close to the 42SiCr steel (Fig. 5). This is evidence that the surface layers of this steel have been heated above the A_3 temperature during the deposition process. Subsequent quicker cooling then resulted in the bainitic microstructure of the interface.

3.1.2 Hybrid parts with post-processing heat treatment

The procedures of quenching and tempering at 250 °C led to a martensitic microstructure in 42SiCr steel. The microstructure of MS1 maraging steel closely resembled the microstructure of solution-annealed AM maraging steel [4]. The tempering temperature was too low to produce visible microstructure change, such as further precipitation or austenite reversion, even though previous EBSD study of the heat treated MS1 steel suggested a slight increase of grain size after solution annealing and tempering at this low temperature [13].

Further heat treatment schedules involved a higher tempering temperature of 490 °C and various holding times. The recommended precipitation hardening procedure for AM maraging steel is heating at 490 °C for 6 h. Since higher tempering temperatures reduce the strength of 42SiCr, these conditions were taken as the upper limit of the tested processes. Above this limit, heat treatment would not improve the tensile strength of the hybrid part, as mechanical properties of the AM maraging steel quickly deteriorate after overaging [13]. Both heat treatments at 490 °C produced lath martensite in the maraging steel. Additionally, the particles of reverted austenite (RA) were observed with increasing precipitation temperature and time in the maraging steel in sample 4-QT-490 °C/6 h. They can be seen as white dots and thin white elongated islands at lath boundaries (Fig. 6h). On

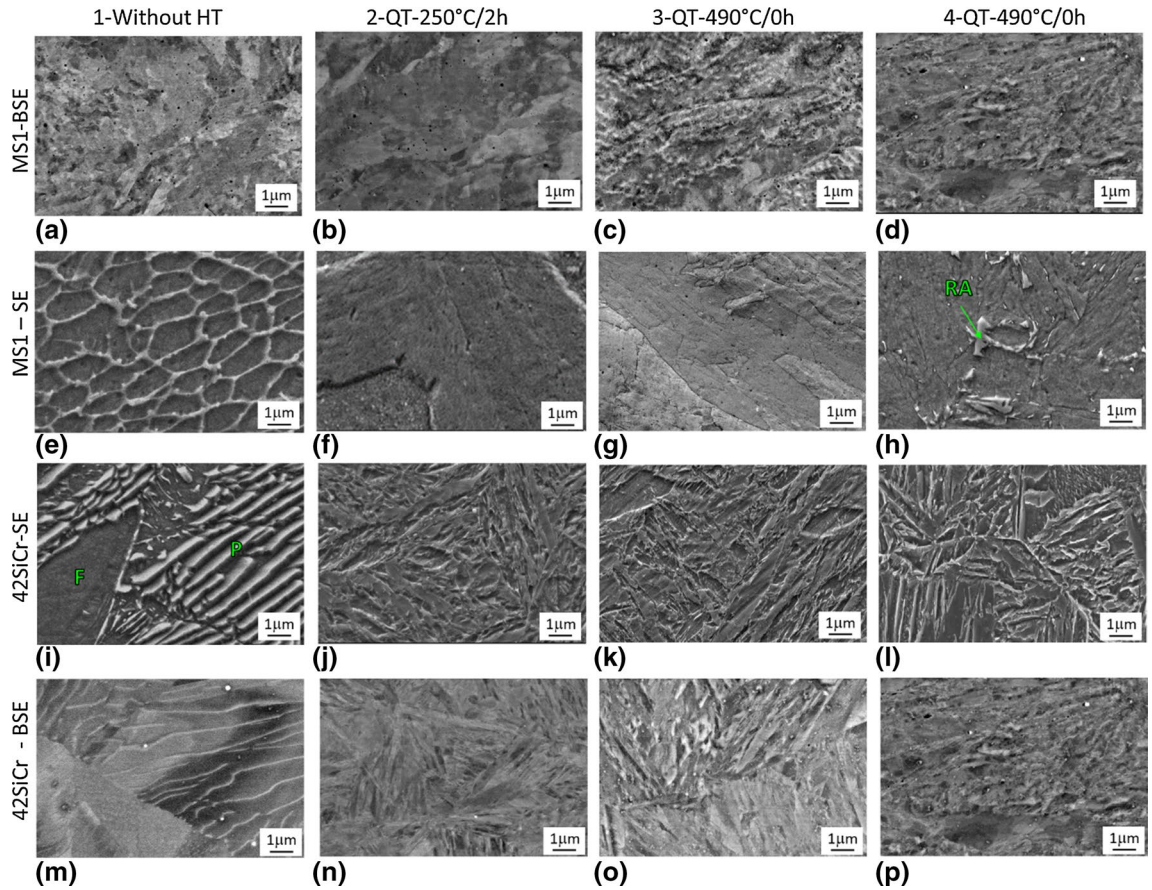

Fig. 6 Microstructure of the hybrid parts 1-without HT (**a**, **e**, **i**, **m**), 2-QT-250 °C/2 h (**b**, **f**, **j**, **n**), 3-QT-490 °C/0 h (**c**, **g**, **k**, **o**) and 4-QT-490 °C/6 h (**d**, **h**, **l**, **p**). The maraging steel microstructure (**a**–**h**), 42SiCr microstructure (**i**–**p**). Reverted austenite (RA) after precipitation at 450 °C/20 min (**g**) and 490 °C/6 h (**h**). Ferrite (F) and pearlite (P) in the initial microstructure of 42SiCr steel

the other hand, fine, but very few, islands of austenite are found in the microstructure of the sample which was brought to 490 °C and not held at the temperature (3-QT-490 °C/0 h, Fig. 6g). In this part, the time was insufficient for significant austenite transformation. In 42SiCr steel, tempered martensite was produced by quenching and tempering. Judging the state of precipitation from the micrographs of etched martensite may not be completely reliable, particularly for finer particles, and, therefore, images of unetched samples observed in BSE are provided as well for all samples. There were increasing signs of carbide precipitation with increasing tempering temperature and times (Fig. 6n–p) in 42 SiCr steel (Fig. 6n–p). In the case of the AM maraging steel, the particles are visible already in the as-built sample without heat treatment and their amount increases only at a precipitation temperature of 490 °C. The sequence of precipitation in this maraging steel was described previously [26] and later confirmed in [13], where first we expect the formation of Ni_3Ti particles, which might gradually change into more complex Ni_3 (Ti, Mo, Al) particles and finally, the Fe–Mo-based particles appear during the over-aging treatments.

3.1.3 Interface of hybrid parts after post-processing heat treatment

Very complex microstructures formed at the 42SiCr-MS1 interface after various heat treatments (Fig. 7a–f), similar to those seen in the as-fabricated part. There was local variation in the chemical composition (Fig. 8a–h). A notable feature of the interface was the relatively frequent occurrence of particles, predominantly in regions where the chemical composition was closer to the maraging steel, i.e. with high Ni, Co, Mo and Ti contents (Fig. 7g, h, i). The particles had increased Mo and Si levels (Fig. 8i–l). Normally, these particles do not form in either steel upon tempering. They were found nowhere else in the hybrid part, apart from the interface. Therefore, it could be assumed that these particles were formed in places where a suitable combination of alloying elements from both steels locally allowed the creation of these particles. As these particles were not found in the reference as-fabricated sample (Fig. 5d–f), it could be concluded that they were formed during post-processing heat treatment. They probably form as early as the austenization and quenching step because they already existed in the sample which underwent tempering at only 250 °C, and they

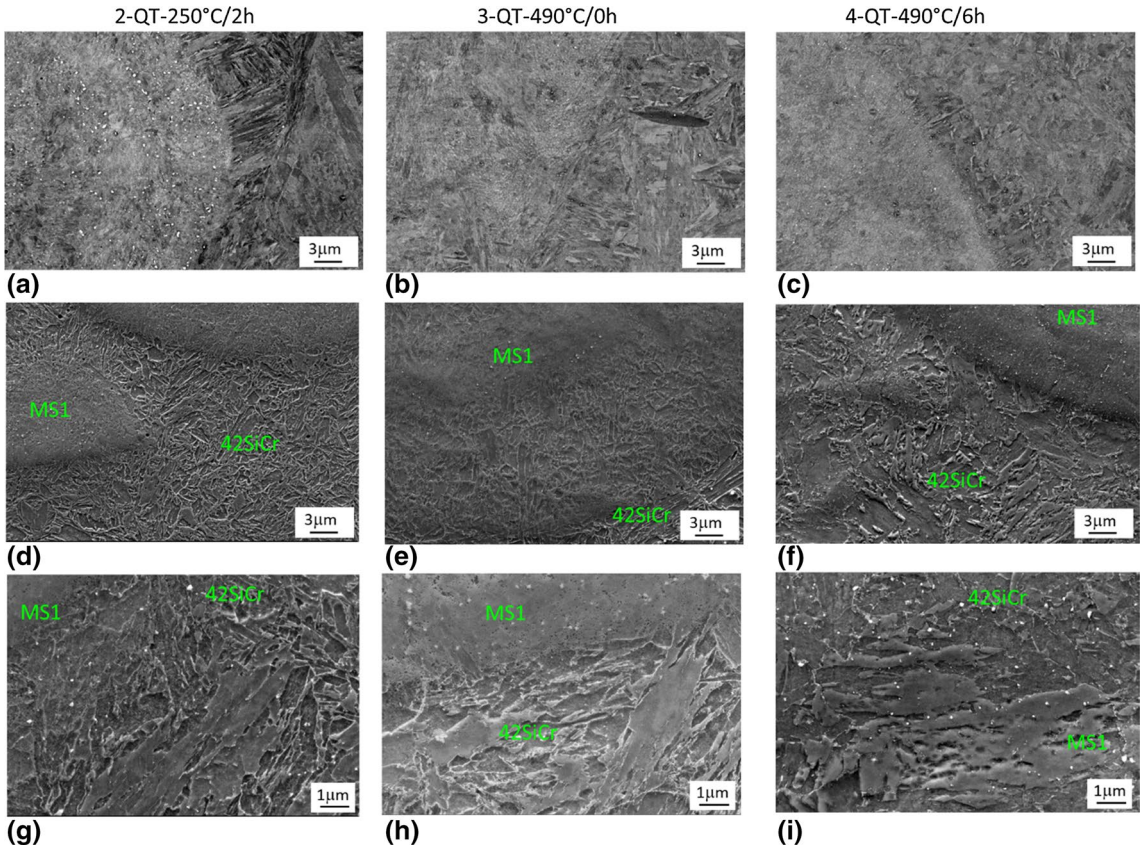

Fig. 7 Interface region of samples 2-QT-250 °C/2 h (**a**, **d**, **g**), 3-QT-490 °C/0 h (**b**, **e**, **h**) and 4-QT-490 °C/6 h (**d**, **f**, **i**), documented in BSE at polished surfaces (**a**–**c**) and in SE at etched surfaces (**d**–**i**) with lower (**d**–**f**) and higher magnification 10,000× (**g**–**i**)

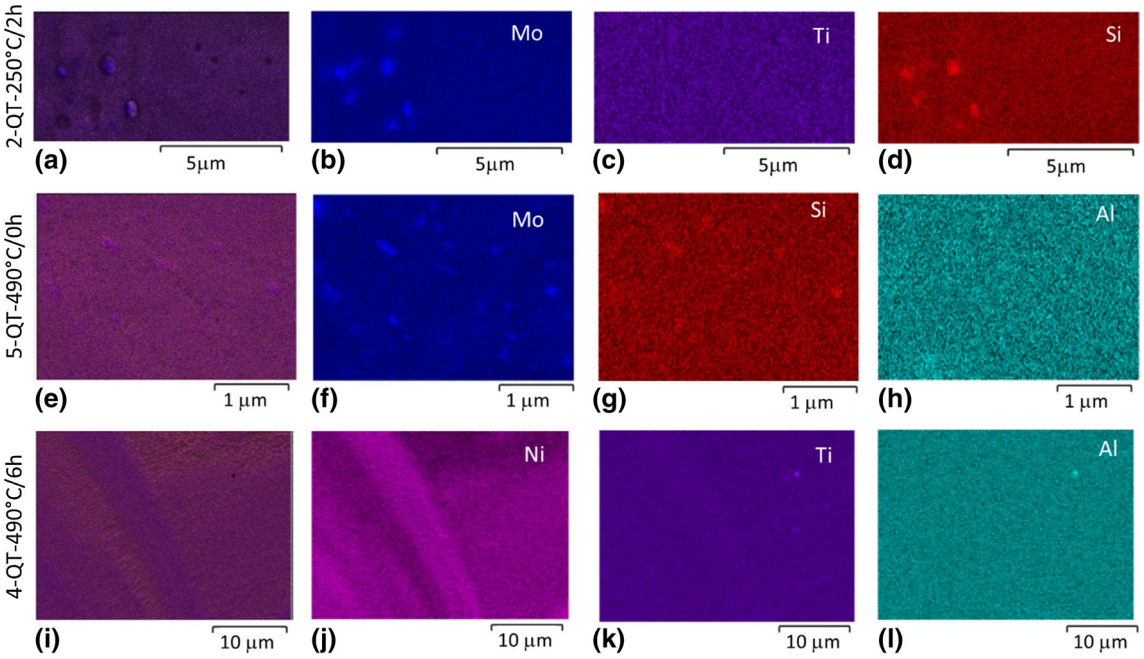

Fig. 8 Identification of Mo–Si particles in part 2-QT-250 °C/2 h (**a**–**d**), identification of particles with increased Mo and Si contents after heat treatment in part 3-QT-490 °C/0 h (**e**–**h**), local distribution of alloying elements in the interface and Ti–Al particle in part 4-QT-490 °C/6 h (**i**–**l**)

did not visibly grow in size or frequency with increasing tempering temperature.

In areas where the chemical composition was closer to 42SiCr steel, very fine carbide precipitates were found at lath boundaries in hybrid parts with post-processing heat treatment. This precipitation became slightly more intensive with increasing tempering temperatures and times (Fig. 7f).

Gradual changes in chemical composition across the interface can be seen in EDS line-scans (Fig. 9). For the samples without heat treatment and tempered at 250 °C, the levels of the main alloying elements in 42SiCr steel (Cr, Mn and Si) drop within a distance of about 150 µm. Then the levels of Cr and Si continue to decrease rather slowly for another 50 µm. This means that higher Si levels can be present even in areas where the chemical composition is closer to that of the maraging steel, which is in accordance with the precipitation of Mo–Si particles mentioned above. At the same time, the concentration of the main alloying elements of the maraging steel (Ni, Co, Mo, Ti) increases across a total distance of about 400 µm. The increase is rather steep across the first 150 µm and slows down significantly as the distance increases from the interface. On the other hand, the samples with the hold at 490 °C show more linear distribution of alloying elements across the interface. Comparison between the line-scans and corresponding micrographs shows that the microstructural changes at the interface are only visible in a layer approximately 50 µm thick, whereas the thickness of the actual region affected by diffusion and detected by EDS was in fact about 400 µm (Fig. 9).

3.1.4 EBSD analysis

EBSD analysis was performed on all samples in three regions: the interfaces and the AM maraging steel and 42SiCr steel (Fig. 10). Both base materials were examined in areas at a safe distance of several millimetres from the interface and from the heat-affected zone. The microstructure of the AM maraging steel without post-process heat treatment was rather fine (Fig. 10a), while 42SiCr steel had a very coarse microstructure (Fig. 10c). Some of the grains were nearly polygonal, but most had a non-specific shape. There was a distinctive refinement of the AM steel in the first deposited layers at the interface (Fig. 10b, e, h, k).

After all quenching and tempering heat treatments, the microstructure of the conventionally produced 42SiCr steel consisted of tempered martensite. The coarsening of the martensite laths could be seen after 6 h of tempering at 490 °C (Fig. 10l), while the sample only heated to 490 °C (Fig. 10i) had similar martensite morphology as the sample after 2 h tempering at 250 °C (Fig. 10f). Fine laths of this martensite in the base material can be seen in the EBSD images (Fig. 10l, f).

In all samples, the microstructure of the maraging steel is very fine at the interface, with larger laths of martensite further away from the interface (Fig. 10a, d, g, j). The refinement in the first deposited layer can be attributed to the faster cooling of the melt pool which was close to the bulk 42SiCr substrate. All the subsequent layers were deposited on preheated earlier layers of MS1, resulting in a slight coarsening

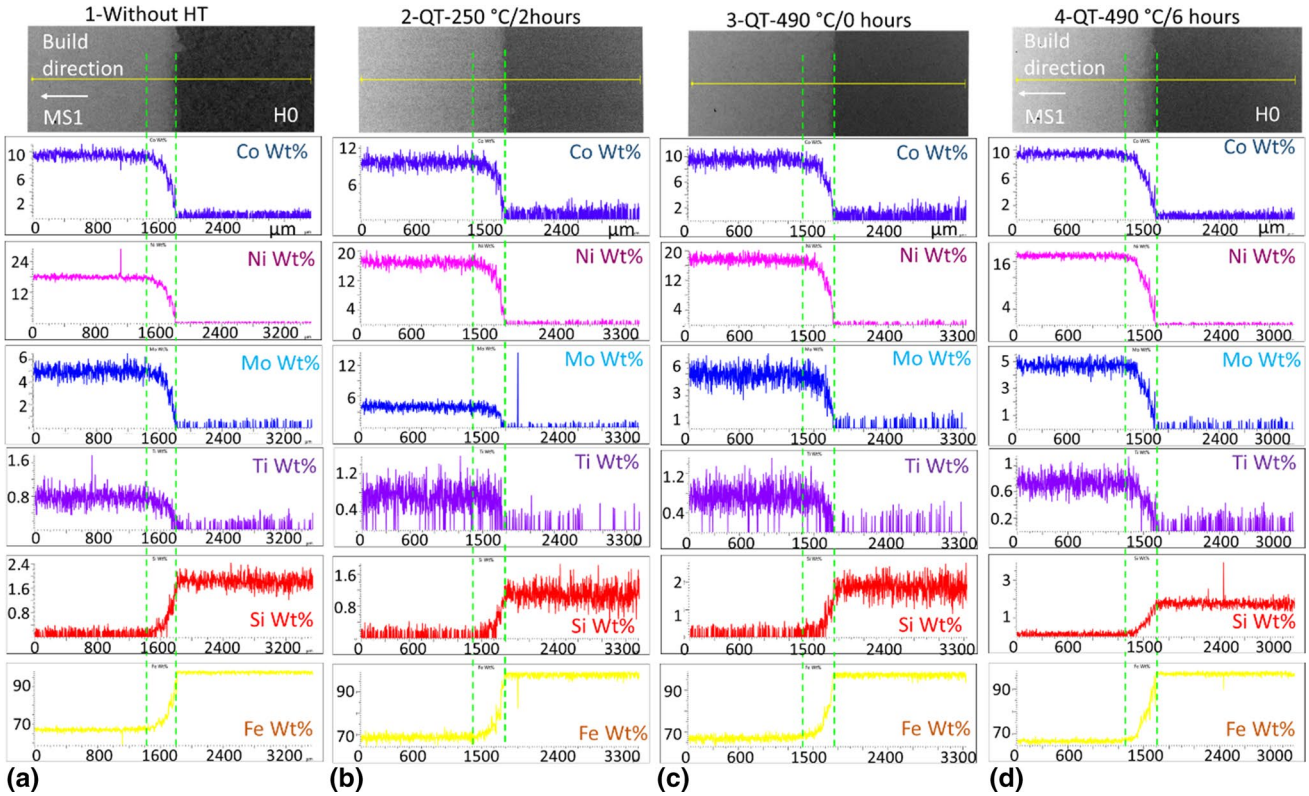

Fig. 9 Changing concentrations of alloying elements across the interface and relationship to the microstructure in sample **a** 1-without HT, **b** 2-QT-250/2 h, **c** 3-QT-490/0 h, **d** 4-QT-490/6 h

of the microstructure. The same coarsening effect was also observed at the MS1-H13 interface in [29]. The microstructure of the maraging steel after all the QT processes (Fig. 10d, g, j) was coarser than the microstructure in the as-fabricated condition (Fig. 10a), which is due to the soaking process at 900 °C.

3.2 Hardness

Macro-hardness HV10 was measured and evaluated separately for each side of the hybrid part. Average values obtained for the three measurements are given in Table 3 (in Sect. 3.3). Microhardness profiles across the interface were obtained from an array of imprints, i.e. a hardness map (Fig. 11), and from linear measurement (Fig. 12). Hardness maps provide more relevant information about local hardness, whereas line measurement offers better visualisation of hardness values for individual measured locations. The position of the 42SiCr-MS1 interface identified from light micrographs is marked by a vertical dashed line in the hardness-line measurement plot in Fig. 12. Four hybrid samples were chosen for the microhardness mapping: one with a higher hardness of 42SiCr steel (2-QT-250 °C/2 h), one with a higher hardness of the maraging steel (4-QT-490 °C/6 h), one which had an equal hardness in both steels (3-QT-490 °C/0 h) and a reference sample without heat treatment (1-without HT). Even though the microhardness was measured on polished samples, the samples with imprints were later etched (Fig. 11e–h) to enable a better correlation of the microhardness maps with the microstructure at the interface.

The microhardness profile was consistent with the hardness values for the individual materials. The reference sample without heat treatment reached higher hardness on the side with MS. Post-process heat treatments at the low tempering temperature of 250 °C led to the highest values of hardness in 42SiCr steel. Additionally, the hardness of the maraging steel was very similar to the hardness in the as-fabricated part (Table 3, Fig. 12).

The heat treatment which resulted in very similar values of hardness in both steels was the precipitation hardening at 490 °C and zero holding time (Fig. 11b). Once this temperature was reached in the central part of the samples, the samples were cooled (3-QT-490 °C/0 h). This procedure was sufficient to obtain a hardness of just below 500 HV0.1 for both steels, suggesting the precipitation hardening of AM steel occurred even during the short heating. Short thermal exposure also had a positive effect on the high hardness retention of the martensitic steel 42SiCr. The hardness map and line measurements show that the peak hardness was reached

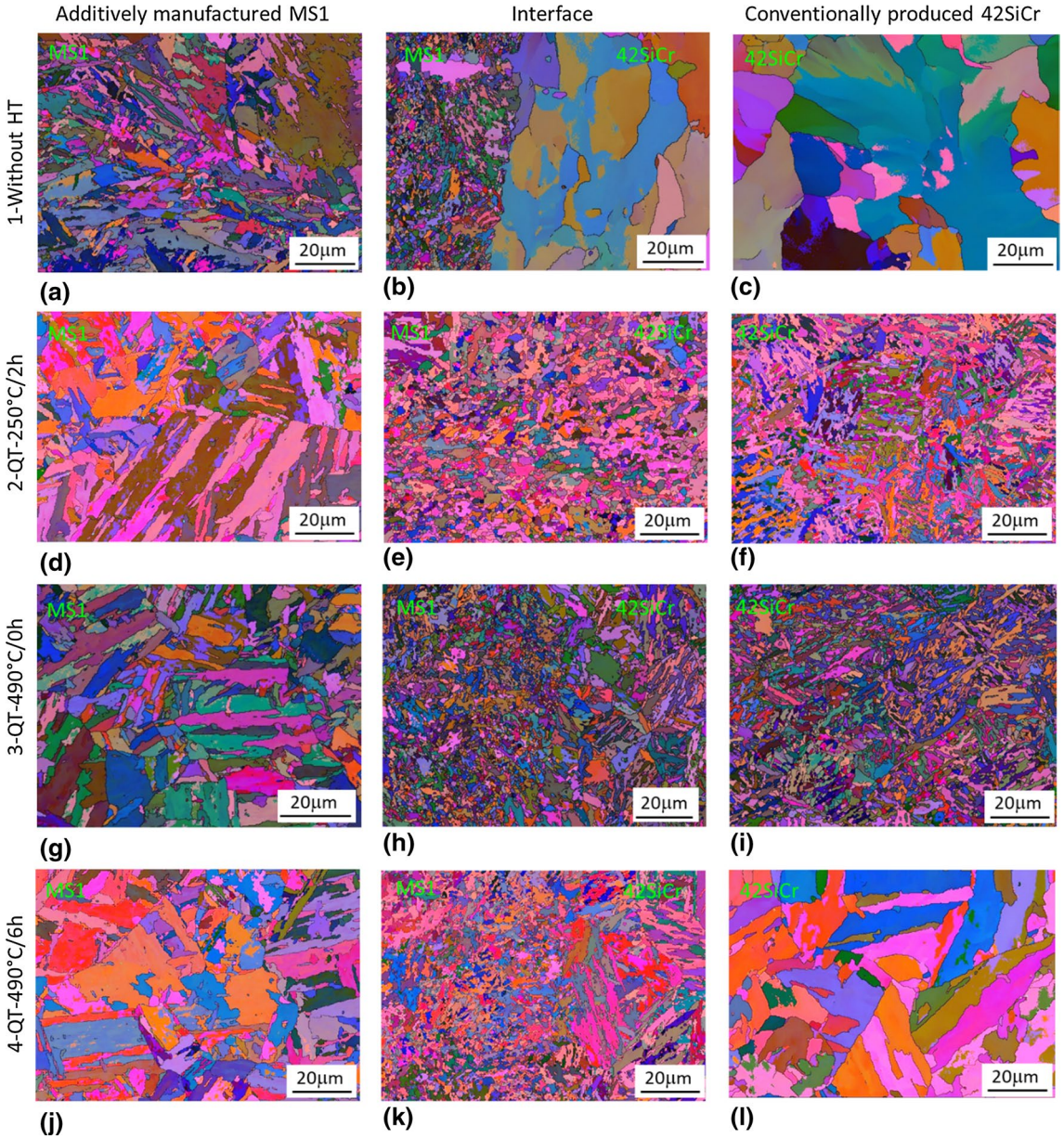

Fig. 10 EBSD analysis (Euler maps) of the reference hybrid part 1-without HT (**a**–**c**), 2-QT-250 °C/2 h (**d**–**f**), 3-QT-490 °C/0 h (**g**–**h**) and 4-QT-490 °C/6 h (**j**–**l**). The images show the interface area (**b**, **e**, **h**, **k**), and base materials—maraging steel MS1 (**a**, **d**, **g**, **j**), and 42SiCr steel (**c**, **f**, **i**, **l**) away from the interface

in the first deposited layers of the maraging steel (marked with a red ellipse in Fig. 11c, g). Outside these layers, hardness dropped in the heat-affected zones on both sides of the interface. The first layer is rather specific, as it is produced on the surface of the cold block of 42SiCr steel, while subsequent layers are deposited on the warmer previous layers. This could result in the quicker cooling of the first layer than for the rest of the part, causing its higher hardness. A long hold at 490 °C (sample 4-QT-490 °C/6 h, Fig. 11c, f) had a different effect on each steel. The maraging steel underwent intensive precipitation, which led to hardening, whereas 42SiCr steel softened due to the tempering of the original martensite.

3.3 Tensile testing

A wide range of mechanical properties was achieved in the hybrid parts (Fig. 13, Table 3). Yield tensile strengths (YTS) were in the range of 738 MPa to 1402 MPa, ultimate tensile strengths (UTS) reached 1025 MPa to 1483 MPa and total elongation (TE) was 9% to 15%. Low uniform elongations (Ag) of 1% to 3% were found in all the hybrid parts.

Table 3 Mechanical properties of hybrid parts (tested on cylindrical samples) and mechanical properties of individual steels (tested on mini-samples)

Sample	YTS [MPa]	UTS [MPa]	TE [%]	Ag [%]	HV10 [–]
Hybrid part 1-without HT	738 ± 26	1065 ± 5	15 ± 0	3 ± 0	–
42SiCr steel—1	492 ± 10	847 ± 0	34 ± 1	19 ± 0	258
Maraging steel—1	840 ± 28	1043 ± 2	23 ± 0	2 ± 0	330
Hybrid part 2-QT-250 °C/2 h	965 ± 13	1065 ± 7	13 ± 0	1 ± 0	–
42SiCr steel—2	1560 ± 12	1869 ± 6	18 ± 0	4 ± 0	595
Maraging steel—2	822 ± 1	969 ± 3	22 ± 0	2 ± 0	322
Hybrid part 3-QT-490 °C/0 h	1402 ± 2	1483 ± 0	10 ± 0	1 ± 0	–
42SiCr steel—3	1424 ± 19	1648 ± 14	17 ± 0	4 ± 0	495
Maraging steel—3	1341 ± 29	1435 ± 6	17 ± 2	2 ± 0	465
Hybrid part 4-QT-490 °C/6 h	1319 ± 1	1409 ± 0	11 ± 0	3 ± 0	–
42SiCr steel—4	1276 ± 11	1397 ± 4	18 ± 0	5 ± 0	452
Maraging steel—4	1865 ± 14	1926 ± 7	11 ± 1	1 ± 0	577

YTS yield tensile strength, *UTS* ultimate tensile strength, *TE* total elongation, *Ag* uniform elongation, *HV* Vickers hardness, 10 kg load

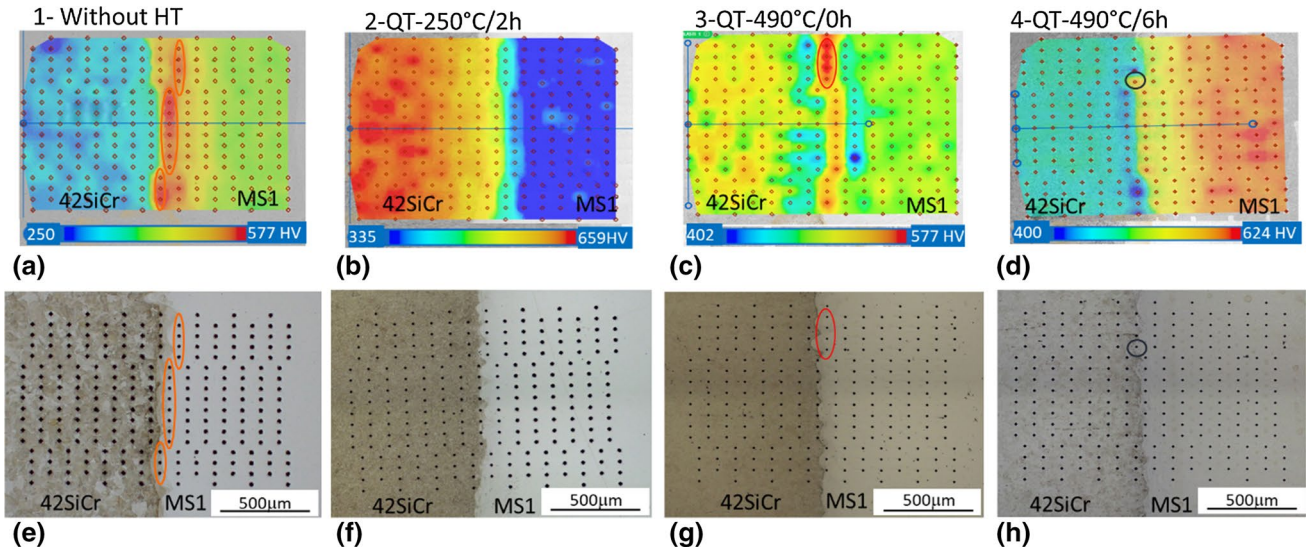

Fig. 11 Hardness map (**a**–**d**) and corresponding layout of imprints (**e**–**h**) on samples 1-without HT (**a**, **e**) 2-QT-250 °C/2 h (**b**, **f**), 3-QT-490 °C/0 h (**c**, **g**) and 4-QT-490 °C/6 h (**d**, **h**)

Hybrid parts with no post-process heat treatment and those treated at a low tempering temperature of 250 °C had lower tensile strengths, slightly above 1000 MPa. Their highest elongation was 12% to 15%. The hardness of the maraging steel was about 330 HV 10 for all these hybrid parts, whereas the hardness of the 42SiCr steel varied from 258 HV 10 (no heat treatment) to 550 to 590 HV 10 after quenching and partitioning or low-temperature tempering. This trend was also reflected in the tensile properties of the mini-samples of both steels. On the other hand, untreated 42SiCr steel had the lowest tensile strength of 847 MPa and the highest elongation of 34%. As-fabricated maraging steel had a tensile strength of 1043 MPa with 23% elongation. Mechanical properties of the entire hybrid parts without heat treatment were close to the properties expected in as-fabricated maraging steel [4]. Both the QP process and QT with tempering at 250 °C significantly increased the tensile strength of 42SiCr steel to 1739 MPa and 1869 MPa, reducing elongation to 21% and 18%, respectively. The tensile strength of the maraging steel in both cases decreased to 910 MPa and 969 MPa without any substantial change in elongation. In the samples 1-without HT and 2-QT-250 °C/2 h, the mechanical properties of the hybrid parts matched the properties of the maraging steel. However, the excellent strength of 42SiCr steel did not contribute to the improvement of the mechanical properties of the hybrid part in these cases.

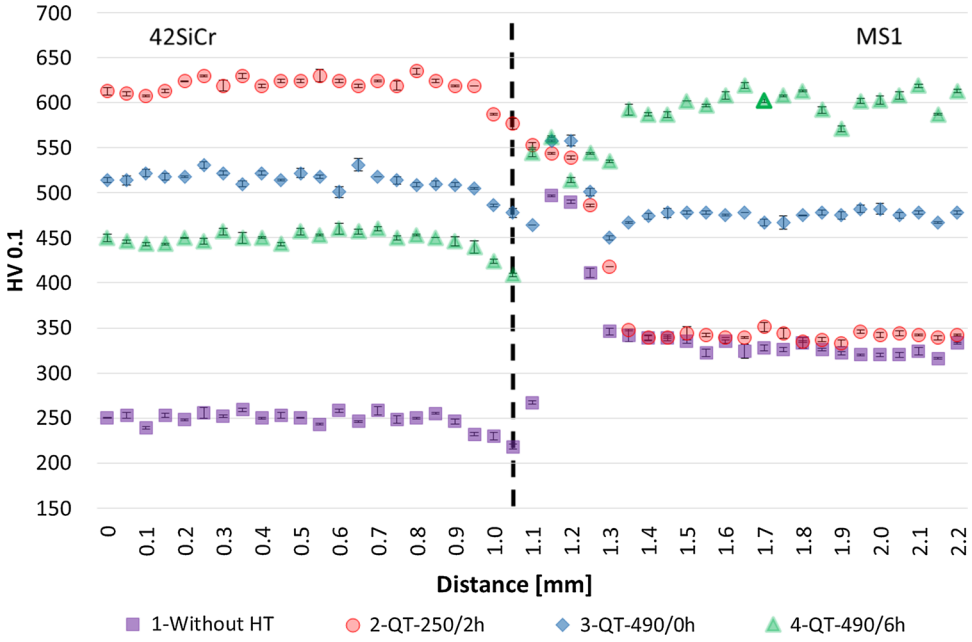

Fig. 12 Line measurements of hardness in samples 1-without HT, 2-QT-250 °C/2 h, 3-QT-490 °C/0 h and 4-QT-490 °C/6 h

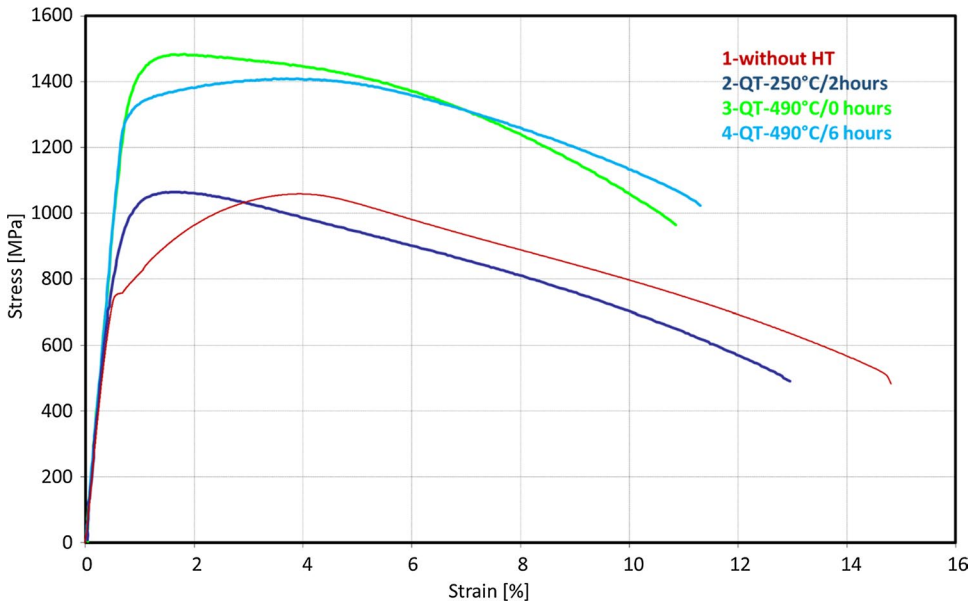

Fig. 13 Typical stress–strain curves from tensile tests of hybrid samples

The yield and tensile strengths of the hybrid parts increased with increasing tempering temperatures, in line with the increasing strengths of the maraging steel. The strength of 42SiCr steel steadily declined with increasing tempering of quenched martensite. The gap between the strengths of both steels narrowed with increasing tempering temperature.

This gap was the smallest in the hybrid part 3-QT-490 °C/0 h, which also provided the best combination of mechanical properties: yield strength of 1400 MPa, tensile strength of 1480 MPa and 10% elongation. The difference between the hardness of 42SiCr and maraging steel was a mere 30 HV10. However, a 6-hour hold at the tempering temperature of 490 °C (4-QT-490 °C/6 h) caused a drop in the strength of 42SiCr steel to 1397 MPa, which is related to the more intensive tempering of the martensite and corresponding cementite precipitation along the lath boundaries of the martensite. At the same time, this caused a very significant increase in the tensile strength of the maraging steel to 1926 MPa, which is connected with the precipitation hardening of the soft matrix by intermetallic particles. Due to the lower strength of 42SiCr steel, this hybrid part 4-QT-490 °C/6 h had approximately 80-MPa lower yield

and tensile strengths than hybrid part 3-QT-490 °C/0 h and fractured in its weaker 42SiCr part.

3.4 Fracture analysis

Similar to conventional welds and joints, interfaces in hybrid parts created by AM could become weak points and initiation sites of failure. Furthermore, a few researchers studying AM hybrid parts or joints have reported fractures located at the interface and argued that this was caused by steep chemical or microstructural gradients in this region [14, 15]. Yet it has been demonstrated on a CMnAlNb steel—MS1 hybrid part that a high-quality interface can eliminate the problems resulting from these gradients. In such cases, the fracture may be located simply in the weaker material instead of the interface or heat-affected zones. This observation agrees with the assumption presented in [39] where the interface failure of an AM 316SS-INC718 part was attributed to the presence of printing defects, such as unmelted particles and pores in the interface. The same finding was made in MS1-H13 bimetals studies [29] and in our work, as shown in the accompanying macrographs taken after tensile testing (Fig. 14).

All the hybrid parts in this study failed in the base materials (Fig. 14g–i). Most of them in the maraging steel, which had lower tensile strength than 42SiCr steel in most cases. One exception was the 4-QT-490 °C/6 h sample where the fracture occurred in the softer 42SiCr steel side. This fracture was not associated with the interface or the heat-affected zones. However, unlike the other fractures, it had a brittle appearance with many secondary radial cracks (Fig. 14c, f). Samples 2-QT-250 °C/2 h and 3-QT-490 °C/0 h suffered cup and cone ductile fracture with dimples (Fig. 14a, b, d, e). More extensive plastic deformation in the central part and more pronounced shear lips were found in the 2-QT-250 °C/2 h sample which also showed deeper and broader

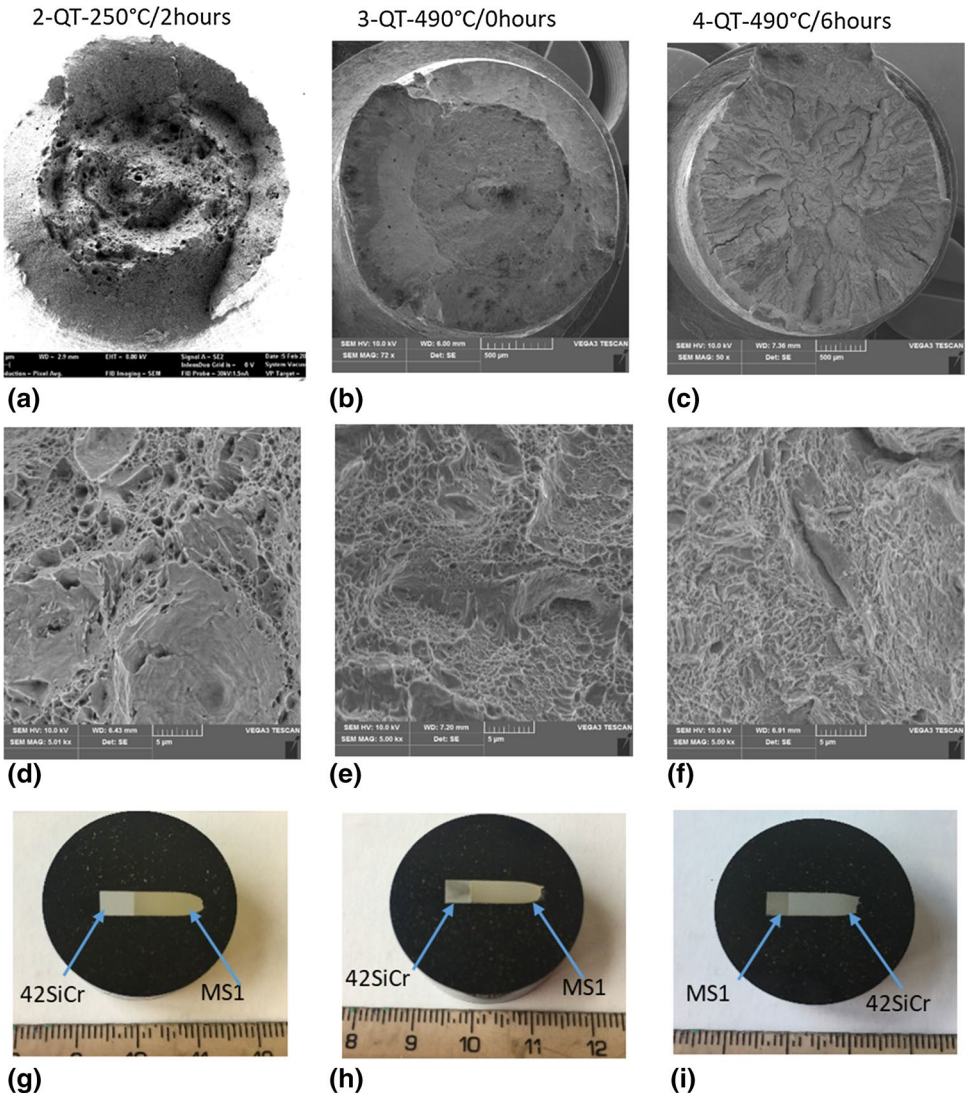

Fig. 14 Fracture surfaces: macrographs (**a**–**c**) and detail SE micrographs (**d**–**f**) of the fracture and location of the fracture within the hybrid part (**g**–**i**). Samples 2-QT-250 °C/2 h (**a**, **d**, **g**), 3-QT-490 °C/0 h (**b**, **e**, **h**) and 4-QT-490 °C/6 h (**c**, **f**, **i**)

dimples (Fig. 14a, d). The central part of the fracture surface in the 3-QT-490 °C/0 h sample is smoother and finer with shallower dimples (Fig. 14b, e).

4 Discussion

The results suggest that hybrid parts can exhibit a wide range of mechanical properties depending on the heat treatment parameters. A necessary condition for the practical application of these hybrid parts is the high quality of the interface, without porosity of the additively manufactured steel or other metallurgical defects. This ensures that the failure of the hybrid part does not initiate prematurely during tensile loading in the joint or the heat-affected zones. Instead, all the tested hybrid samples fractured in the base material which had a lower strength after the applied heat treatment.

A new type of Mo–Si particle was observed in the fusion zone, which was not present in the corresponding area of the as-built hybrid part. This suggests that post-process heat treatment was the prerequisite for the precipitation of these Mo–Si particles. They probably form during the first step of the heat treatment (i.e. austenization and quenching), as they were found in the sample which underwent tempering at only 250 °C. Various temperatures and hold times of the tempering step did not visibly affect the size or distribution of the particles. This would correspond to the reported occurrence of Mo_3Si silicides in an AM austenitic stainless steel, where they precipitated at high angle grain boundaries at temperatures around 700 °C to 900 °C, in areas where Mo content locally reached around 4.8 wt.% and Si around 0.8 wt.% [38]. The required contents of Si and Mo could also be present locally in some areas of the MS1-42SiCr interface, supporting the formation of this type of silicide.

The results of interface hardness measurements showed an interesting trend on the MS1 side. In the as-built condition, the hardness of the first layers of MS1 increased in comparison to the rest of the AM part. The hardness of these layers was further slightly increased by the subsequent heat treatment. However, the temperature and time of precipitation did not have a significant effect on the hardness of the first printed layers and only affected the hardness of the base material. This can be explained by two separate contributions to the hardening of the first printed layers. One contribution can be associated with significant grain refinement of the first layers of the printed MS1, which was caused by deposition on a cold substrate. As the printing proceeded, the subsequent layers were deposited on the still warm previous layers of MS1, resulting in an increase of MS1 grain size visible in Fig. 10. This effect would explain the hardness increase in as-built hybrid part 1-without HT.

The area with a specific hardness development on the MS1 side of the interface was around 400 µm wide (Fig. 12), which corresponds to the inter-diffusion interface layer documented by EDS analysis in the corresponding area of the hybrid part (Fig. 9). The second contribution to the hardness of the first layers of MS1 can be, therefore, related to the precipitation of special particles in the diffusion-affected area of MS1, which occurred during heat treatment of the hybrid part. The peak hardness values of MS1 first layers after heat treatment does not seem to depend on the precipitation hardening conditions, as they were the same for 2-QT-250 °C/2 h, 3-QT-490 °C/0 h and 4-QT-490 °C/6 h treatments. These layers belong to the "transition region", where the precipitation of Mo-based particles is already visible after annealing (they were observed in the sample with the lowest hardening temperature 2-QT-250 °C/2 h. This precipitation also contributed to achieving maximum hardness. When heat treatment with parameters optimal for precipitation hardening of MS was applied (4-QT-490 °C/6 h), this transition region did not undergo further hardening (as it did not have the chemical composition of the maraging steel), while the base material reached peak hardness typically obtained at this precipitation temperature.

In as-built conditions, the mechanical properties correspond to the properties of the printed part. 42SiCr had a ferritic-pearlitic microstructure with good ductility, but rather low strength. The shape of the stress–strain curve of the hybrid part 1-without HT reflects the properties of 42SiCr because it has the largest area of uniform deformation, which is not usually seen in maraging steels [40]. Subsequent heat treatments triggered different strengthening mechanisms of the steels. For 42SiCr steel, the maximum strength and hardness could be obtained by simple quenching, which would produce a martensitic microstructure. Obtained martensite is, however, quite brittle and has a tendency to cracking and, therefore, low-temperature annealing at 250 °C was applied to optimise the strength-to-ductility balance. The same heat treatment did not, however, result in the strengthening of MS1 steel. During the first step of the heat treatment, the coarsening of the matrix was achieved due to a relatively high temperature of 900 °C, which supported not only recrystallization of the printed microstructure, but also some subsequent grain growth. The grain size distribution was more homogeneous after heat treatment than in the as-built condition, where there were coarser grains with a large number of extremely fine grains formed at the grain borders.

Precipitation strengthening did not occur during the second step of heat treatment, as the temperature of 250 °C was too low. This steel shows significant strengthening only after longer holds at temperatures in an interval of approximately 450–500 °C [13], even though slight strengthening was already observed after 6 h holding at 350 °C [13]. The opposite effect can be observed in 42SiCr steel, where higher precipitation temperatures and longer holds supported tempering. The resulting decrease of the strength of

the martensitic matrix was, however, not fully compensated by the precipitation of cementite.

Overall, the trends in the mechanical properties of both steels suggest that hybrid parts with even better tensile strength than 3-QT-490 °C/0 h could be obtained by heat treatment with approximately 1-h tempering at 490 °C. This would balance the strengths of both steels, increasing the strength of AM steel while causing only a smaller drop in the strength of 42SiCr steel. Still, the mechanical properties achieved in this study can be considered a success compared with the MS1-H13 hybrid part [29]. H13 is also a martensitic chromium-alloyed medium-carbon tool steel with around 5% chromium, 1.5% molybdenum and 1% vanadium. Despite the elevated content of alloying elements in comparison to 42SiCr steel, a hybrid part of conventional H13 and AM-fabricated MS1 only achieved an ultimate tensile strength of 600 MPa [29]. This comparison highlights the importance of developing optimal post-process heat treatments for hybrid parts.

5 Conclusions

Additive manufacturing of maraging steel on medium-carbon 42SiCr martensitic steel was performed using selective laser melting. Hybrid parts built in this way were then heat-treated to optimise their mechanical properties, by quenching and tempering, with tempering temperatures from 250 to 490 °C. Whereas quenching and tempering at 250 °C improved the mechanical properties of 42SiCr steel significantly, the properties of the entire hybrid part did not improve when compared to the as-fabricated condition. This was because the maraging steel only obtained the same properties as in the solution-annealed condition, i.e. without any precipitation hardening effect. Heat treatments that involved higher tempering temperatures promoted precipitation hardening in the maraging steel but also softening of 42SiCr steel due to the tempering of the martensite. An optimal combination of mechanical properties in both steels was obtained by quenching and subsequent very short tempering at 490 °C. This treatment produced the best mechanical properties of the hybrid part: 1483 MPa tensile strength and 10% elongation. Even higher strength might be expected after approximately 1-h tempering at 490 °C based on the trends in the mechanical properties of both steels in response to tempering.

Two contributions to the hardness increase of the first layers of MS1 were observed. One is associated with grain refinement during the printing of the first layers on the cold substrate. The second contribution is related to the precipitation of special particles in the diffusion-affected area of the first layers on the MS1 side during the heat treatment of the hybrid part and will, therefore, only become apparent after annealing.

In all these hybrid parts, fracture occurred in the base materials and not in the interface or the heat-affected zones. This shows that the joint need not be a critical region in a hybrid part, provided that the high quality and purity of the interface is maintained.

Acknowledgements This contribution has been prepared within the project ITI CZ.02.1.01/0.0/0.0/18_069/0010040, "Research of additive technologies for future application in mechanical engineering practice—RTI plus" under the auspices of the National Sustainability Programme I of the Ministry of Education, Youth and Sports of the Czech Republic aimed at supporting research, experimental development and innovation.

Author contributions Conceptualization: LK, ŠJ, IZ. Methodology: LK, IZ, ŠJ. Formal analysis and investigation: LK, KB. Writing—original draft preparation: LK. Writing—review and editing: LK, KB. Resources: IZ, ŠJ. Supervision: LK. Visualisation: LK.

Declarations

Conflict of interest The authors have no competing interests to declare that are relevant to the content of this article.

Ethics approval All ethical requirements of the journal are met. This article does not contain any studies with human participants or animals performed by any of the authors.

Consent to participate All authors agree to be the author of the publication.

Consent for publication All authors agree to submit their publications to this journal.

References

1. Bhardwaj T, Shukla M. Effect of scan direction on tensile properties and fractography of laser additive manufactured maraging steel. Mater Today Proc. 2019;18:3842–8. https://doi.org/10.1016/j.matpr.2019.07.323 (**Part 72019**).
2. Oter ZC, Gencer Y, Tarakci M. Microstructure evolution and surface quality of laser-sintered maraging steel parts produced on different building platform positions. Optik. 2020;202:163568. https://doi.org/10.1016/j.ijleo.2019.163568.

3. Shamsdini SAR, Shakerin S, Hadadzadeh A, Amirkhiz BSh, Mohammadi M. A trade-off between powder layer thickness and mechanical properties in additively manufactured maraging steels. Mater Sci Eng A. 2020;776:139041. https://doi.org/10.1016/j.msea.2020.139041.
4. Kučerová L, Zetková I, Jandová A, Bystrianský M. Microstructural characterisation and in-situ straining of additive-manufactured X3NiCoMoTi 18-9-5 maraging steel. Mater Sci Eng A. 2019;75018:70–80. https://doi.org/10.1016/j.msea.2019.02.041.
5. Sanjari M, Hadadzadeh A, Pirgazi H, Shahriari A, Amirkhiz BS, Kestens LAI, Mohammadi M. Selective laser melted stainless steel CX: role of built orientation on microstructure and micromechanical properties. Mater Sci Eng A. 2020;786:139365. https://doi.org/10.1016/j.msea.2020.139365.
6. Lu QY, Nguyen NV, Hum AJW, Tran T, Wong CH. Identification and evaluation of defects in selective laser melted 316L stainless steel parts via in-situ monitoring and micro computed tomography. Addit Manuf. 2020;35:101287. https://doi.org/10.1016/j.addma.2020.101287.
7. Saboori A, Aversa A, Marchese G, Biamino S, Lombardi M, Fino P. Microstructure and mechanical properties of AISI 316L produced by directed energy deposition-based additive manufacturing: a review. Appl Sci. 2020;10:3310. https://doi.org/10.3390/app10093310.
8. Monková K, Zetková I, Kučerová L, et al. Study of 3D printing direction and effects of heat treatment on mechanical properties of MS1 maraging steel. Arch App Mech. 2018;89:791–804. https://doi.org/10.1007/s00419-018-1389-3.
9. Henry TC, Phillips FR, Cole DP, Garboczi E, Haynes RA, Johnson T. In situ fatigue monitoring investigation of additively manufactured maraging steel. Int J Adv Manuf Tech. 2020;107:3499–510. https://doi.org/10.1007/s00170-020-05255-4.
10. Ansell TY, Ricks JP, Park C, Tipper CS, Luhrs CC. Mechanical properties of 3D-printed maraging steel induced by environmental exposure. Metals. 2020;10:218. https://doi.org/10.3390/met10020218.
11. Hadadzadeh A, Shahriari A, Amirkhiz BS, Li J, Mohammadi M. Additive manufacturing of an Fe–Cr–Ni–Al maraging stainless steel: Microstructure evolution, heat treatment, and strengthening mechanisms. Mater Sci Eng A. 2020;78710:139470. https://doi.org/10.1016/j.msea.2020.139470.
12. Conde FF, Escobar JD, Oliveira JP, Jardini AL, Avila JA. Austenite reversion kinetics and stability during tempering of an additively manufactured maraging 300 steel. Addit Manuf. 2019;29:100804. https://doi.org/10.1016/j.addma.2019.100804.
13. Kučerová L, Burdová K, Jeníček Š, Chena I. Effect of solution annealing and precipitation hardening at 250–550 °C on microstructure and mechanical properties of additively manufactured 1.2709 maraging steel. Mater Sci Eng A. 2021;814:141195. https://doi.org/10.1016/j.msea.2021.141195.
14. Azizi H, Ghiaasiaan R, Prager R, Ghoncheh MH, Phillion AB. Metallurgical and mechanical assessment of hybrid additively-manufactured maraging tool steels via selective laser melting. Addit Manuf. 2019;27:389–97. https://doi.org/10.1016/j.addma.2019.03.025.
15. Cyr E, Asgari H, Shamsdini S, Purdy M, Hosseinkhani K, Mohammadi M. Fracture behaviour of additively manufactured MS1-H13 hybrid hard steels. Mater Lett. 2018;212:174–7. https://doi.org/10.1016/j.matlet.2017.10.097.
16. Kučerová L, Zetková I, Jeníček Š, Burdová K. Hybrid parts produced by deposition of 18Ni300 maraging steel via selective laser melting on forged and heat treated advanced high strength steel. Addit Manuf. 2020;32:101108. https://doi.org/10.1016/j.addma.2020.101108.
17. Ahsan MRU, Tanvir ANM, Seo G-J, Bates B, Kim DB. Heat-treatment effects on a bimetallic additively-manufactured structure (BAMS) of the low-carbon steel and austenitic-stainless steel. Addit Manuf. 2020;32:101036. https://doi.org/10.1016/j.addma.2020.101036.
18. Bhaduri D, Penchev P, Essa K, Dimov S, Pullini D. Evaluation of surface/interface quality, microstructure and mechanical properties of hybrid additive-subtractive aluminium parts. CIRP Ann. 2019;68:237–40. https://doi.org/10.1016/j.cirp.2019.04.116.
19. Ambrogio G, Gagliardi F, Muzzupappa M, Filice L. Additive-incremental forming hybrid manufacturing technique to improve customised part performance. J Manuf Process. 2019;37:386–91. https://doi.org/10.1016/j.jmapro.2018.12.008.
20. Hirtler M, Jedynak A, Sydow B, Sviridov A, Bambach M. A study on the mechanical properties of hybrid parts manufactured by forging and wire arc additive manufacturing. Procedia Manuf. 2020;47:1141–8. https://doi.org/10.1016/j.promfg.2020.04.136.
21. Bambach M, Sizova I, Sydow B, Hemes S, Meiners F. Hybrid manufacturing of components from Ti-6Al-4V by metal forming and wire-arc additive manufacturing. J Mater Process Technol. 2020;282:116689. https://doi.org/10.1016/j.jmatprotec.2020.116689.
22. Meiners F, Ihne J, Jürgens P, Hemes S, Weisheit A. New hybrid manufacturing routes combining forging and additive manufacturing to efficiently produce high performance components from Ti-6Al-4V. Procedia Manuf. 2020;47:261–7. https://doi.org/10.1016/j.promfg.2020.04.215.
23. Khodabakhshi F, Farshidianfar MH, Bakhshivash S, Gerlich AP, Khajepour A. Dissimilar metals deposition by directed energy based on powder-fed laser additive manufacturing. J Manuf Process. 2019;43:83–97. https://doi.org/10.1016/j.jmapro.2019.05.018.
24. Rashkovets M, Mazzarisi M, Nikulina AA, Casalino G. Analysis of laser direct stainless steel powder deposition on Ti6Al4V substrate. Mater Lett. 2020;2741:128064. https://doi.org/10.1016/j.matlet.2020.128064.
25. Abe T, Sasahara H. Dissimilar metal deposition with a stainless steel and nickel-based alloy using wire and arc-based additive manufacturing. Precis Eng. 2016;45:387–95. https://doi.org/10.1016/j.precisioneng.2016.03.016.
26. Tian Y, Shen J, Hu S, Wang Z, Gou J. Microstructure and mechanical properties of wire and arc additive manufactured Ti-6Al-4V and AlSi5 dissimilar alloys using cold metal transfer welding. J Manuf Process. 2019;46:337–44. https://doi.org/10.1016/j.jmapro.2019.09.006.
27. Ahire PG, Patil US, Kadam MS. Genetic algorithm based optimization of the process parameters for manual metal arc welding of dissimilar metal joint. Procedia Manuf. 2018;20:106–12. https://doi.org/10.1016/j.promfg.2018.02.015.
28. Wippermann A, Gutowskia TG, Denkena B, Dittrich M-A, Wessarges Y. Electrical energy and material efficiency analysis of machining, additive and hybrid manufacturing. J Clean Prod. 2020;251:119731. https://doi.org/10.1016/j.jclepro.2019.119731.
29. Shakerin S, Hadadzadeh A, Amirkhiz BS, Shamsdini S, Li J, Mohammadi M. Additive manufacturing of maraging steel-H13 bimetals using laser powder bed fusion technique. Addit Manuf. 2019;29:100797. https://doi.org/10.1016/j.addma.2019.100797.
30. Tan C, Zhou K, Ma W, Min L. Interfacial characteristic and mechanical performance of maraging steel-copper functional bimetal produced by selective laser melting based hybrid manufacture. Mater Des. 2018;155:77–85. https://doi.org/10.1016/j.matdes.2018.05.064.
31. Kučerová L, Aišman D, Jirková H, Mašek B, Hauserová D. Optimization of Q-P Process Parameters with Regard to Final Microstructures and Properties. In: Annals of DAAAM for 2009

& Proceedings of the 20th international DAAAM symposium. Vienna: DAAAM International, 2009. Pp 1035–1036, ISSN: 1726–9679
32. Speer JG, Streicher AM, Matlock DK, Rizzo F, Krauss G. Quenching and partitioning: a fundamentally new process to create high strength trip sheet microstructures. In: Austenite formation and decomposition. 2003, pp 505–522.
33. Pashangeh S, Somani MC, Ghasemi-Banadkouki SS, Kamiri-Zarchi HR, Kaikkonen P, Porter DA. On the decomposition of austenite in a high-silicon medium-carbon steel during quenching and isothermal holding above and below the Ms temperature. Mater Charact. 2020;162:110224. https://doi.org/10.1016/j.matchar.2020.110224.
34. Cai HL, Chen P, Oh JK, Wu D, Yi HL. Quenching and flash-partitioning enables austenite stabilization during press-hardening processing. Scr Mater. 2020;178:77–81. https://doi.org/10.1016/j.scriptamat.2019.10.047.
35. Kozłowska A, Radwański K, Matus K, et al. Mechanical stability of retained austenite in aluminum-containing medium-Mn steel deformed at different temperatures. Arch Civ Mech Eng. 2021;21:19. https://doi.org/10.1007/s43452-021-00177-8.
36. Kučerová L, Jirková H, Hauserová D, Mašek B. Comparison of microstructures and properties obtained after different heat treatment strategies of high strength low alloyed steel. J Iron Steel Res Int. 2011;18(Supplement 1–1):427–31.
37. Opatová K, Zetková I, Kučerová L. Relationship between the size and inner structure of particles of virgin and re-used MS1 maraging steel powder for additive manufacturing. Materials. 2020;13(4):956. https://doi.org/10.3390/ma13040956.
38. Houshang Y, Miao S, Pu D, Lin L, Prorok BC, Xiaoyuan L. Thermal stability and microstructural evolution of additively manufactured 316L stainless steel by laser powder bed fusion at 500–800 ℃. Addit Manuf. 2021;41:101981. https://doi.org/10.1016/j.addma.2021.101981.
39. Mei X, Wang X, Peng Y, Gu H, Zhong G, Yang S. Interfacial characterization and mechanical properties of 316L stainless steel/inconel 718 manufactured by selective laser melting. Mat Sci Eng A. 2019;758:185–91. https://doi.org/10.1016/j.msea.2019.05.011.
40. Kučerová L, Zetková I, Jeníček Š, Burdová K. Production of hybrid joints by selective laser melting of maraging tool steel 1.2709 on conventionally produced parts of the same steel. Materials. 2021;14:2105. https://doi.org/10.3390/ma14092105.